Geophysical Research Letters

RESEARCH LETTER
10.1029/2024GL111989

Inter-Model Uncertainty in Projecting Precipitation Changes Over Central Asia Under Global Warming

Mengyuan Yao[1,2,3], **Haosu Tang**[4], **and Gang Huang**[1,2,3]

[1]Key Laboratory of Earth System Numerical Modeling and Application, Institute of Atmospheric Physics, Chinese Academy of Sciences, Beijing, China, [2]Laboratory for Regional Oceanography and Numerical Modeling, Qingdao National Laboratory for Marine Science and Technology, Qingdao, China, [3]University of Chinese Academy of Sciences, Beijing, China, [4]Department of Geography, University of Sheffield, Sheffield, UK

Abstract The impact of global warming on Central Asian precipitation suffers from huge uncertainties, yet their origins remain largely unidentified. This study investigates the inter-model spread in the projection of winter Central Asian precipitation (WCAP) using models from the Coupled Model Inter-comparison Project Phase 6. The results reveal a homogenous wetting trend in WCAP, with the primary source of uncertainty in its magnitude stemming from the dynamic component of vertical moisture advection. This dynamical uncertainty is further attributed to an out-of-phase variation between two Eurasian westerly jets, which can enhance the upward motion over Central Asia through positive relative vorticity advection and warm temperature advection. The opposing variation between two westerly jets can be traced to cooling in the North Pacific, which alters jet intensity through changes in the meridional temperature gradient. This study informs policy and adaptation strategies to better cope with future climate shifts in Central Asia.

Plain Language Summary Central Asia (CA) faces high water demand for agriculture and livelihoods, but struggles with scarce precipitation and dry soils. Therefore, accurate simulation and projection of precipitation in CA are crucial. Based on Coupled Model Inter-comparison Project Phase 6 models, this study shows a consistent wetting trend in winter precipitation across CA under global warming, with an 8.84%/K increase projected under the SSP5–8.5 scenario. The moisture budget analysis reveals that the primary source of uncertainty in precipitation projections comes from the dynamic component of vertical moisture transport. The strengthened ascending motion over CA is further attributed to an enhanced Eurasian polar front jet (EAPJ) and a weakened Eurasian subtropical jet (EASJ) through positive relative vorticity advection and warm temperature advection. The intensity changes of these two jets can be traced back to cooling in the North Pacific, which results in dipole meridional temperature gradient (MTG) changes over CA. Negative (positive) MTG changes in northern (southern) CA enhance (reduce) the mean-state MTG and increase (decrease) upper-level zonal winds according to the thermal wind relation, thereby intensifying (weakening) the EAPJ (EASJ). This study advances the understanding of uncertainties in precipitation projection and informs policymakers on addressing water shortages in the climate-sensitive CA.

Key Points:

- Winter precipitation projections over Central Asia exhibit substantial inter-model uncertainty in the magnitude of the wetting trend
- This uncertainty in precipitation projection is primarily driven by the dynamic component of vertical moisture advection
- The dynamical uncertainty is attributed to the out-of-phase variation between two westerly jets, which is traced to North Pacific cooling

Supporting Information:

Supporting Information may be found in the online version of this article.

Correspondence to:

H. Tang and G. Huang,
haosu.tang@sheffield.ac.uk;
hg@mail.iap.ac.cn

Citation:

Yao, M., Tang, H., & Huang, G. (2024). Inter-model uncertainty in projecting precipitation changes over central Asia under global warming. *Geophysical Research Letters*, *51*, e2024GL111989. https://doi.org/10.1029/2024GL111989

Received 14 AUG 2024
Accepted 4 DEC 2024

Author Contributions:

Conceptualization: Haosu Tang
Data curation: Mengyuan Yao
Formal analysis: Mengyuan Yao, Haosu Tang
Funding acquisition: Gang Huang
Investigation: Mengyuan Yao
Methodology: Mengyuan Yao, Haosu Tang
Project administration: Gang Huang
Software: Mengyuan Yao
Supervision: Gang Huang
Validation: Mengyuan Yao
Visualization: Mengyuan Yao
Writing – original draft: Mengyuan Yao
Writing – review & editing: Haosu Tang, Gang Huang

1. Introduction

Central Asia (CA), comprising Uzbekistan, Tajikistan, Turkmenistan, Kyrgyzstan, and Kazakhstan, is the largest arid and semi-arid region in the Northern Hemisphere, with an average annual precipitation of less than 300 mm (Guo et al., 2021). Despite its arid climate, limited precipitation, and infertile soils, CA has one of the world's highest per capita water consumption rates, largely due to its dependence on agriculture. Even more concerning is the fact that the economic return on water use in this region is lower than anywhere else on the planet (Varis, 2014). These factors make CA particularly vulnerable and sensitive to the impacts of climate change (Peng et al., 2019; Ranasinghe et al., 2019). Therefore, accurately simulating and projecting the impacts of climate change on CA are essential. Such projections will be critical for the irrigated agricultural economy and human health in the region (Yu et al., 2021), playing a vital role in guiding climate change adaptation efforts and regional strategic planning.

An unprecedented warming trend has occurred in CA during the past four decades, outpacing both global and Northern Hemisphere average warming rates (Masson-Delmotte et al., 2021; Zhang et al., 2019). As temperatures rise, the atmosphere's water-holding capacity increases, leading to a more active hydrological cycle (Folland et al., 2001; Qiu et al., 2024). Several studies have examined the responses of future precipitation in CA to global

warming. For example, projections indicate less precipitation in central and southern CA, particularly in summer, but an increase of winter precipitation in the northern and eastern regions (Lioubimtseva & Henebry, 2009). Wu et al. (2013) revealed that while the precipitation is expected to decrease over the Pamir Plateau, it will increase across the rest of CA. Additionally, rising temperatures are expected to intensify the seasonality of CA's precipitation as well, shifting the first peak from summer to spring in its northern regions (Jiang, Zhou, Chen, & Zhang, 2020). Huang et al. (2014) suggested that future precipitation will likely increase across most of CA, though only half of the models agree, with the rest predicting decreasing trends, including strong aggregated drought (Yao et al., 2021). Despite advancements in the Coupled Model Intercomparison Project Phase 6 (CMIP6), which aimed at overcoming the shortcomings of CMIP5 (such as overestimating annual and seasonal precipitation) (Rivera & Arnould, 2020), significant uncertainties and inconsistencies in projected precipitation over CA persist. For instance, models tend to overestimate monthly precipitation from October to May in central CA deserts, and they struggle to accurately capture the annual cycle in northern CA (Guo et al., 2021). Huang et al. (2014) also found that precipitation uncertainties increased as emissions decreased in CMIP5. Notably, even models from the same institute can significantly differ in their performance when reproducing long-term precipitation trends (Guo et al., 2021). Some models project greater aridity in the future, while others suggest less, highlighting the significance of inherent natural variability in the projection for arid zones (Lioubimtseva & Cole, 2006). Therefore, it is urgent to identify the sources of these projected precipitation uncertainties in CA and work toward constraining them.

The two leading upper-tropospheric westerly jet streams in the Northern Hemisphere, namely the Eurasian subtropical jet (EASJ) and Eurasian polar front jet (EAPJ), significantly influence weather and climate in the Eurasian continent (Liu et al., 2022; Pang et al., 2023; Yin & Zhang, 2021). Previous studies have found that precipitation in CA is consistently modulated by the location and strength of the EASJ, which affects moisture fluxes and embedded weather disturbances (Bothe et al., 2011; Chen et al., 2008; Schiemann et al., 2008). Additionally, the EASJ can induce upper-level divergence, thereby contributing to precipitation in CA (Wang & Huang, 2011). Enomoto (2004) highlighted that the EASJ facilitates the propagation of quasi-stationary Rossby waves, which can affect other regions through the propagation of perturbation kinetic energy and convective motion forcing. This Silk-Road teleconnection wave train along the EASJ could influence the Eurasian atmospheric circulation, further affecting precipitation and temperature events (Yao et al., 2024; Zhang et al., 2020). The position and strength of the EASJ can be influenced by sea surface temperature (SST) anomalies in various oceans. For instance, changes in the EASJ's position over CA are primarily related to SST anomalies in the Indian Ocean and tropical eastern Pacific, while changes in its strength are associated with anomalies in the North Pacific (Xu et al., 2024; Zhao et al., 2018; Zhou et al., 2019). To illustrate, warming tropical Atlantic and North Pacific contribute to the weakened EASJ, whereas ESPJ tends to shift northward (Liu et al., 2024). Meanwhile, the cooling over Northwestern Pacific results in a weakened EAPJ and an enhanced EASJ through the SST-related dipole meridional temperature gradient (MTG) pattern across the Eurasian Continent (Liu et al., 2022). Compared to the EASJ, the EAPJ is closely associated with cold air activity in high latitudes and affects atmospheric baroclinicity in mid-to-high latitudes (Hall et al., 2015; Pang et al., 2023). Lee and Kim (2003) further revealed that the EAPJ strengthens when the EASJ weakens, possibly driven by the northward shift of baroclinic wave growth in the mid-latitudes.

Given the imbalance between scarce precipitation and high water consumption in CA, accurate projections of precipitation are crucial for adapting to ongoing climate change. However, projections of future precipitation changes in CA demonstrate remarkable inter-model spread, and the origins of these discrepancies remain largely unidentified. In this study, we use the multi-model ensemble mean (MME) as a basis to understand the inter-model spread and investigate changes in boreal winter CA precipitation winter Central Asian precipitation (WCAP) from December to February. This season is selected due to its larger inter-model uncertainties compared to other seasons. Our primary goal is to identify the origins of model uncertainty among CMIP6 models for WCAP projections. To this end, this study attempts to address the following questions: (a) How consistent are CMIP6 models in projecting WCAP changes, and what are the inter-model spreads among them? (b) What are the primary sources of uncertainty in WCAP projections among CMIP6 models? (c) What underlying physical processes ultimately contribute to the inter-model spread of WCAP projections? These results will be essential for developing effective climate adaptation strategies and ensuring sustainable water resource management in the vulnerable and climate-sensitive CA.

2. Data and Methods

2.1. Observational and Model Data

We use the monthly precipitation data set from the Global Precipitation Climatology Center (GPCC) monthly product version 2022 (Schneider et al., 2022), as well as the high-resolution gridded data sets from the Climatic Research Unit (CRU) and the University of Delaware (Udel) precipitation data sets, to evaluate the performance of models in simulating WCAP. These observational data sets cover the period from 1970 to 2014. We examine the first ensemble member (typically "r1i1p1f1") of historical simulations from 25 CMIP6 climate models (detailed in Table S1 in Supporting Information S1), which replicate past climate conditions from 1850 to 2014. These simulations serve as a benchmark for assessing the model's ability to reproduce precipitation in CA. Considering the generally strong reproducibility of these state-of-art models, all of which have spatial correlation coefficients with observations exceeding 0.66, we include them all in the analysis (Figure S1 in Supporting Information S1). Additionally, outputs from the SSP5–8.5 scenario for each model from 2015 to 2100 are adopted for formal analysis. Outputs from the SSP1–2.6, SSP2–4.5, and SSP3–7.0 scenarios are also employed for validation.

2.2. Methods

Before analysis, all observations and model simulations are bilinearly interpolated onto a common 2.5° latitude × 2.5° longitude grid. We target precipitation changes relative to climatology under global warming, defined as the difference between the future (2070–2099 mean) and present-day (1970–1999 mean) climatology. To account for spatial heterogeneity, we express future changes as percentages of precipitation anomalies. These changes are further normalized by the area-weighted global mean of surface temperature changes in each model to eliminate the inter-model uncertainty arising from differences in climate sensitivity. The two-sided Student's *t*-test is employed to assess the significance of inter-model regressions.

3. Results

3.1. Dominant Pattern of WCAP Projection Uncertainty

We first evaluate the performance of WCAP simulations in the CMIP6 historical experiment. Climatologically, the mean-state WCAP features an increasing gradient from north to south based on observational data sets, with the highest values centered in southeastern CA (Figure S1a in Supporting Information S1). This spatial pattern is well captured in the MME (Figure S1b in Supporting Information S1). The spatial correlations between individual models and observations all exceed 0.66, with the CMIP6 MME showing a high correlation of 0.91 (Figure S1c in Supporting Information S1). Hence, the models listed in Table S1 in Supporting Information S1 demonstrate generally good reproducibility in simulating WCAP.

Based on models' simulations, we further analyze the amplitude of precipitation changes in CA across different seasons. The MME of CMIP6 models reveals a wetting trend of 2.88 mm month^{-1} decade^{-1} in CA during winter, persisting from the late 20th into the 21st century under the high-emission SSP5–8.5 scenario (Figure 1a). A similar wetting trend is observed in spring and autumn, although with a less pronounced magnitude, while a drying trend is noted in summer (Figure S2 in Supporting Information S1). Notably, winter exhibits the largest inter-model variability in area-averaged precipitation projections, contrasting with the smaller inter-model spread observed in other seasons.

The homogenous wetting pattern observed across the entire CA is consistently captured by all models, with the area-weighted regional mean intensity in winter reaching up to 8.84%/K (Figure 1b). The wetting pattern during winter is more pronounced compared to other seasons and demonstrates higher spatial consistency across models (Figures S3a–S3c in Supporting Information S1). Meanwhile, the wetting pattern in winter keeps high consistency among different future scenarios (SSP1–2.6, SSP2–4.5, SSP3–7.0; Figure S4 in Supporting Information S1). The WCAP changes derived from individual models suggest that all models exhibit a wetting pattern with a certain degree of spatial similarity to MME, with all spatial correlation coefficients exceeding 0.50 (Figure S5 in Supporting Information S1). Hence, no single model exists the bias that may significantly distort the overall results, indicating that these models are applicable for the analysis.

10.1029/2024GL111989

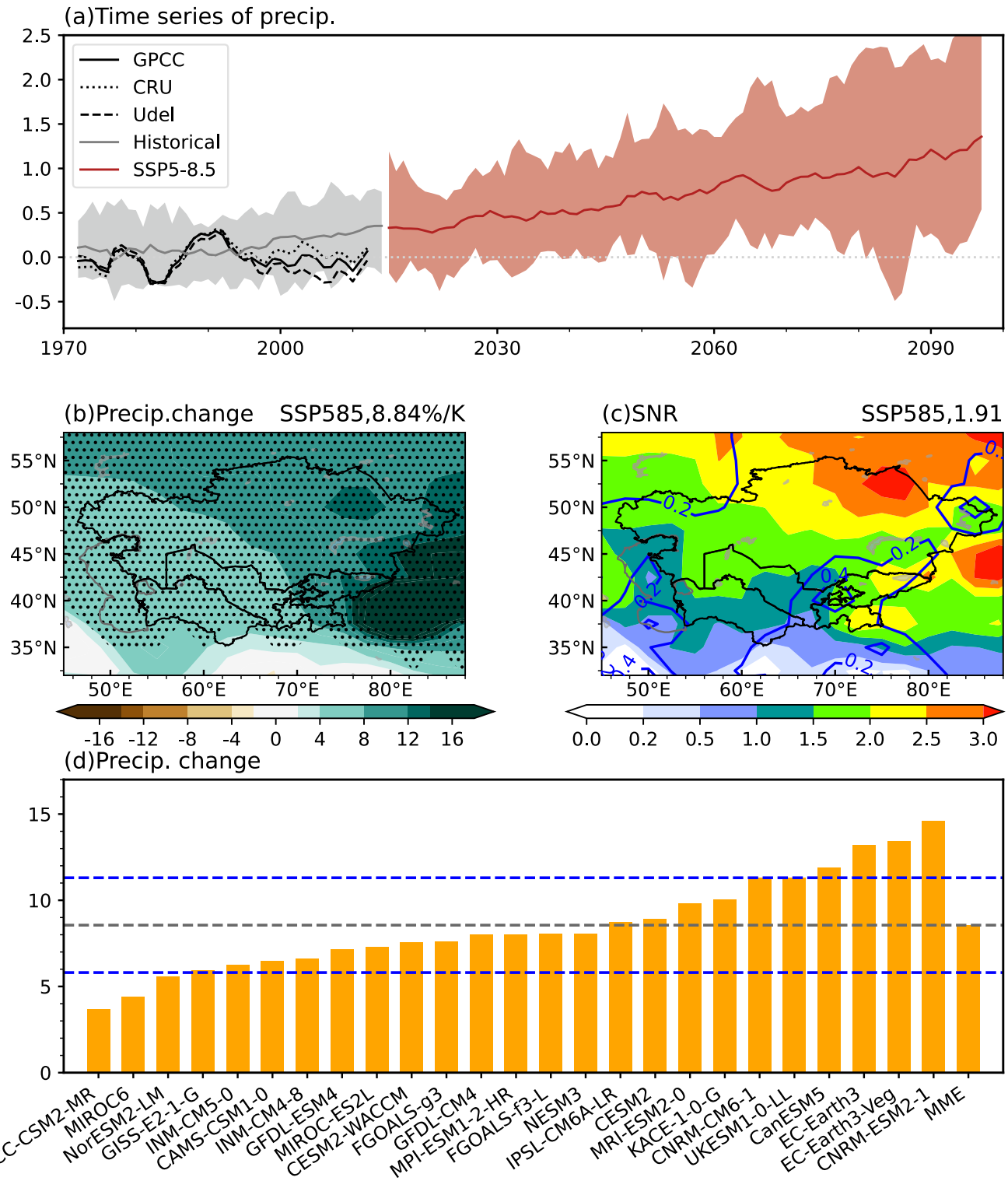

Figure 1. (a) Time series of 5-year running mean winter Central Asian precipitation (WCAP) anomalies (units: mm day^{-1}), relative to the present-day average (1970–1999). Historical (gray) and SSP5–8.5 (red) simulations are shown for the minimum and maximum across 25 models (shading), and the ensemble mean (solid lines). The black solid and dash lines are the three observational series (details in Data). (b) Spatial changes in WCAP (units: % K^{-1}). The dots denote regions where at least 80% of the models agree on the sign of change. (c) The inter-model SNR (shading) and standard deviation (STD) (contour) of projected WCAP changes. (d) Changes in area-weighted regional mean WCAP (units: % K^{-1}) of each model and the ensemble mean. The gray and blue lines indicate the ensemble mean and one STD. The number at upper right in panels (b, c) is the averaged value over CA.

In addition, the first leading mode of WCAP projection, derived from the inter-model Empirical Orthogonal Function analysis, also features a homogenous increasing pattern over CA, accounting for 58.43% of the total variance (Figure S6a in Supporting Information S1). The corresponding principal component exhibits a strong correlation with the projected area-averaged WCAP across models, with a correlation coefficient of 0.86 ($p < 0.01$). This implies that the dominant pattern of WCAP projection uncertainty is robust and not sensitive to the choice of statistical methods.

Despite the generally strong performance of CMIP6 models in reproducing the historical precipitation, considerable deviations in their projections arising from internal variability still exist. The quantified uncertainty of precipitation projection under SSP5–8.5 scenario, measured by the signal-to-noise ratio (SNR, detailed in Text S1 in Supporting Information S1), reveals that the ratio between the absolute value of projected changes and the standard deviation (STD) is seasonally less than 1.5 across most of CA, except in winter when the SNR exceeds 1.5 (Figure 1c and Figure S3 in Supporting Information S1). The higher SNR at each grid in winter may be attributed to the more pronounced wetting trend, despite the STD being of similar magnitude across seasons. Outlier models, with projections exceeding one STD, contribute substantially to the inter-model spread (Figure 1d). Consequently, mid to long-term projections of WCAP exhibit high uncertainty, with the highest projected value being approximately four times the lowest (Figure 1d).

3.2. Physical Processes Underlying the Inter-Model Spread

To further investigate physical mechanisms behind the inter-model spread of precipitation changes under global warming, the moisture budget analysis is performed to quantify the contributions of specific terms to the uncertainty in projected WCAP (detailed in Text S2 in Supporting Information S1). The wetting over CA is primarily attributed to increased vertical moisture transport, supplemented to a less extent by horizontal moisture advection (Figure 2). In contrast, decreased evaporation acts as an opposing force (Figures 2b and 2g). A closer examination of the vertical moisture advection term reveals that the dominant contribution arises from an increase in the dynamic component. This component exhibits a homogeneous wetting pattern, akin to the uncertainty observed in precipitation projections under global warming (Figures 2a and 2f–g). This term is closely associated with intensified ascending motion over the region (Figure 3a). Conversely, the thermodynamic component mainly acts to suppress precipitation changes (Figures 2e and 2g). In summary, the wetting pattern in WCAP changes may primarily be driven by the dynamical component of vertical moisture advection, which is also consistently observed across other scenarios, including SSP 1–2.6, SSP2–4.5 and SSP3–7.0 (Figures S4b, S4d, and S4f in Supporting Information S1). The strengthened vertical motion over CA is associated with changes in the upper-level horizontal circulation (Figure 3b). Specifically, an out-of-phase wind pattern over the active region of the westerly jet suggests an enhanced EAPJ and a weakened EASJ. This configuration promotes negative curvature in CA, leading to the anomalous upper-level high pressure (Figure 3b).

To uncover the main factors affecting the anomalous vertical motion responsible for the dynamic component over CA, we further diagnose it using the quasi-geostrophic vertical pressure velocity equation (detailed in Text S3 in Supporting Information S1). The primary factors contributing to the strengthened ascending motion over CA include anomalous zonal relative vorticity advection (B2) and meridional temperature advection (C4) (Figures S7a, S7c and S7l in Supporting Information S1). The presence of mean-state westerly flow ($\overline{u_g}$) over the whole CA results in positive relative vorticity advection originating from northwestern CA, facilitating intensified ascendance in the region (Figures 3a and 3c). Besides, the decomposition of C4 (500-hPa meridional wind anomaly $v_g{}'$ and mean-state temperature $\overline{T}$) reveals that the warm air transported by anomalous southerly winds across western and central CA is another key factor for the ascendance (Figure 3d).

3.3. Oceanic Origin of Westerly Jet Variations

In tandem with previous studies, we find that variations in the westerly jets may be the primary drivers of projection uncertainty in WCAP (Jiang, Zhou, Wang, et al., 2020; Pang et al., 2023). Here, we further investigate the origins of this out-of-phase variation in the intensity of two westerly jets among CMIP6 models. According to the thermal wind relation, the variation in the jet streams is closely associated with changes in the vertically integrated MTG (Liao & Zhang, 2013). A diploe pattern in MTG changes is observed around CA, with negative MTG changes over northern CA intensifying the mean-state MTG (Figure 4a). The intensified MTG increases upper-level wind speeds, leading to an enhanced EAPJ. Besides, the accelerated winds hinder Arctic cold air from

10.1029/2024GL111989

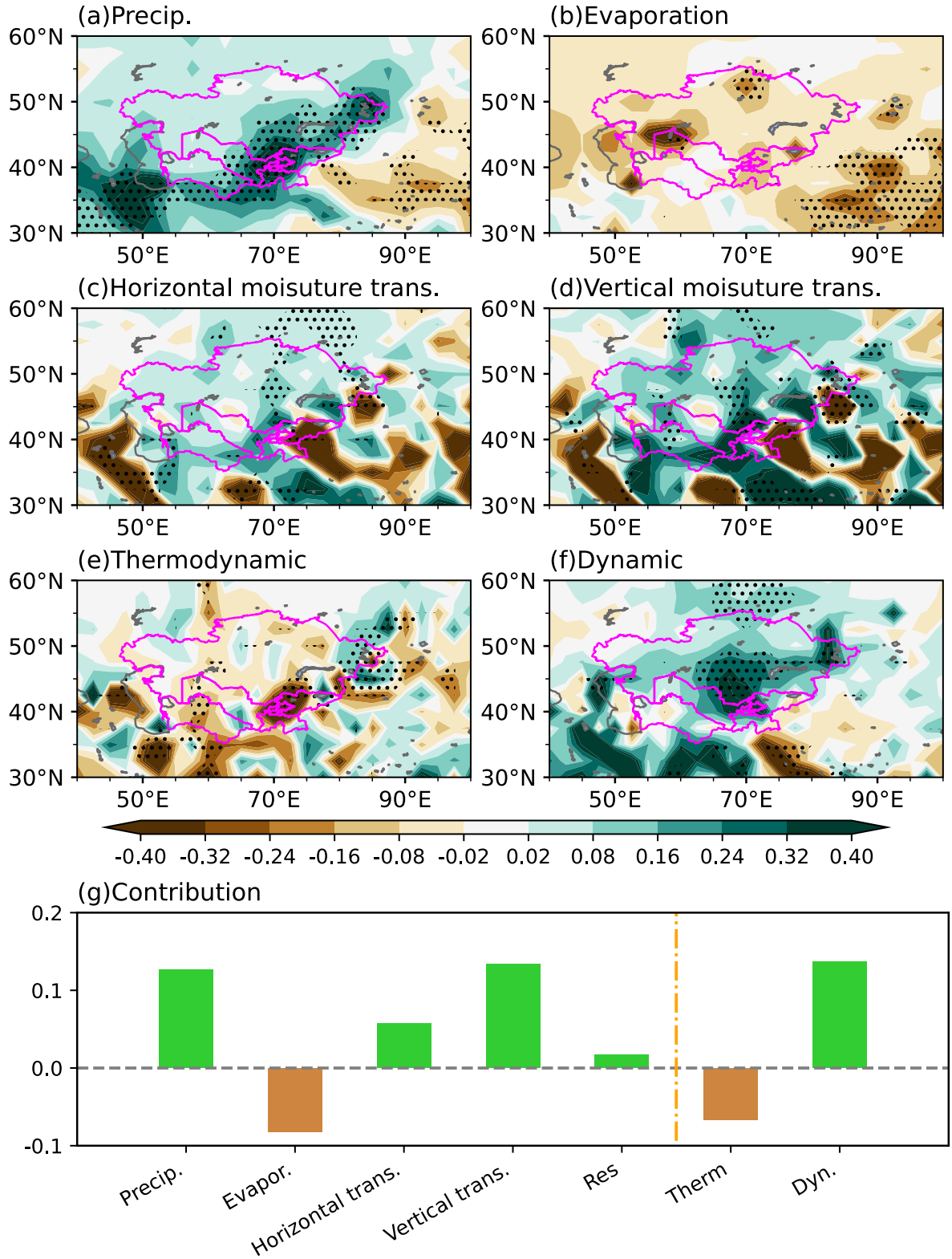

Figure 2. Inter-model regression of changes (units: 10^{-1} mm day^{-1} K^{-1}) in winter (a) precipitation, (b) evaporation, (c) the horizontal moisture advection term, (d) the vertical moisture advection term, and the (e) thermodynamic and (f) dynamic components of the vertical moisture advection term with winter Central Asian precipitation. The solid dots indicate 90% confidence level. (g) CA-averaged contribution of each term in panels (a–f) and the residual.

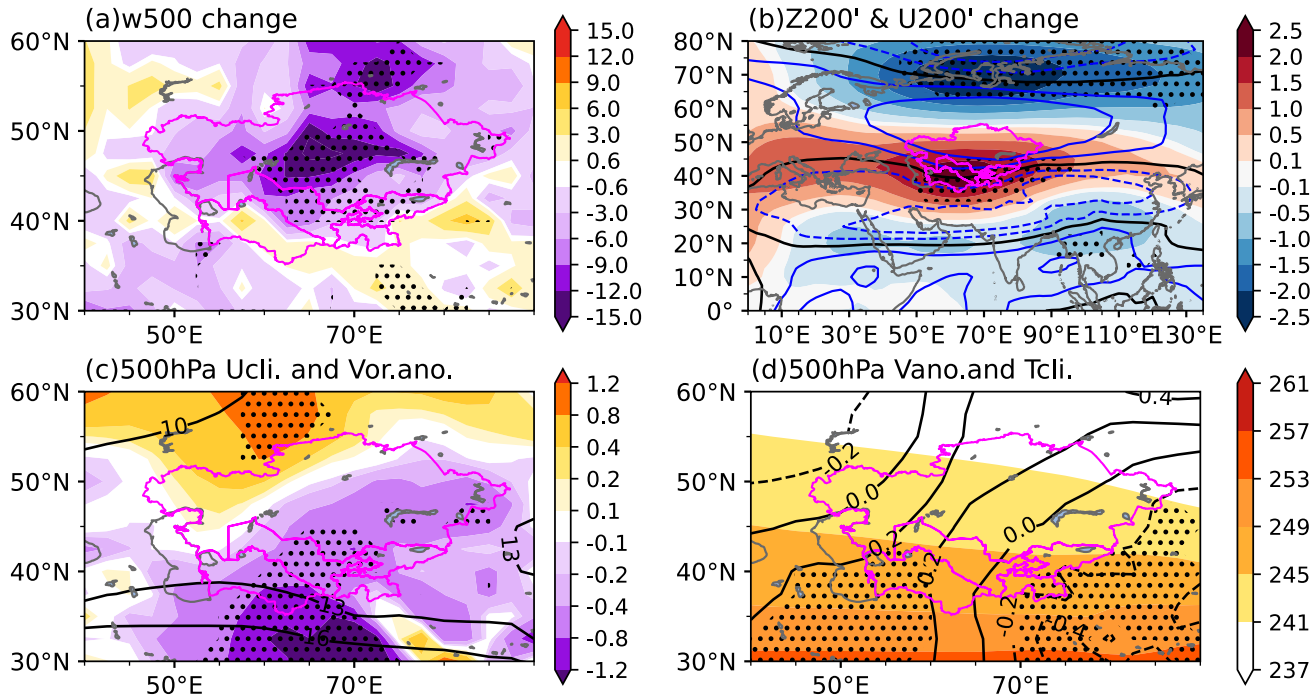

Figure 3. Inter-model regression of changes in winter (a) 500-hPa vertical velocity (units: Pa s^{-1} K^{-1}), (b) 200-hPa eddy geopotential height (units: m K^{-1}, shading) and zonal wind (units: m s^{-1} K^{-1}, contour) with winter Central Asian precipitation (WCAP). The black line indicates the zero value. Solid (dashed) blue lines indicate positive (negative) value with an interval of 0.2. (c) 500-hPa winter mean-state zonal wind ($\overline{u_g}$, units: m s^{-1}, contour) and inter-model regression of changes in relative vorticity anomaly (ξ_g', units: 10^{-6} m s^{-1} K^{-1}, shading) with WCAP. (d) 500-hPa winter mean-state temperature ($\overline{T}$, units: K, shading) and inter-model regression of changes in meridional wind anomaly (v_g', units: m s^{-1} K^{-1}, contour) with WCAP. The solid dots indicate 90% confidence level for variables shaded, except in panel (d) for contours.

propagating south, thereby increasing the atmospheric baroclinicity over northern CA. This increased baroclinicity further enhances warm temperature advection from southern CA and is accompanied by strong ascendance in the troposphere (Figures 3a and 3b).

On the contrary, positive MTG changes over southern CA would reduce the mean-state MTG, leading to a weakening of the EASJ (Figure 4a). The synergistic effect of an intensified EAPJ in the north and a weakened EASJ in the south contributes to upper-level high pressure anomalies and upward motion in CA through positive relative vorticity advection and warm temperature advection. Additionally, the weakening of the EASJ typically results in reduced moisture transport (Jiang, Zhou, Wang, et al., 2020; Jiang & Zhou, 2021), which further explains why the horizontal moisture transport does not dominate the uncertainty of the region's wetting trends. The MTG changes across the Eurasian continent could be attributed to the winter North Pacific SST decadal (NPD) pattern-like cooling over the Northwestern Pacific (Figure 4b). To facilitate further analysis, we define the normalized 9-year running average of regional mean SST changes over the key cold region (145°–180°E, 40°–60°N) as the North Pacific index (NPI) (Liu et al., 2022; Sun et al., 2016). The regression pattern of MTG changes onto the opposite value of NPI bears notable similarities to the pattern of MTG changes regressed onto WCAP (Figure 4c), confirming that the negative phase of the NPD pattern may serve as an important external driver of MTG anomalies. The main conclusions remain robust when the selected region is slightly expanded or contracted. Therefore, the cooling pattern in the North Pacific could trigger an enhanced EAPJ and a weakened EASJ through out-of-phase MTG changes across the Eurasian continent (Figure 4d). The SST-induced MTG changes contribute to the stronger EAPJ that blocks the southward movement of cold air and thereby enhances the negative MTG in CA. This process ultimately increases atmospheric baroclinicity, promoting ascending motion through warm air advection from southern CA.

Our findings indicate that SST anomalies may significantly impact Eurasian westerly jets, thereby influencing the uncertainty in precipitation projections. To trace the origins of cooling SST anomalies in the North Pacific, we

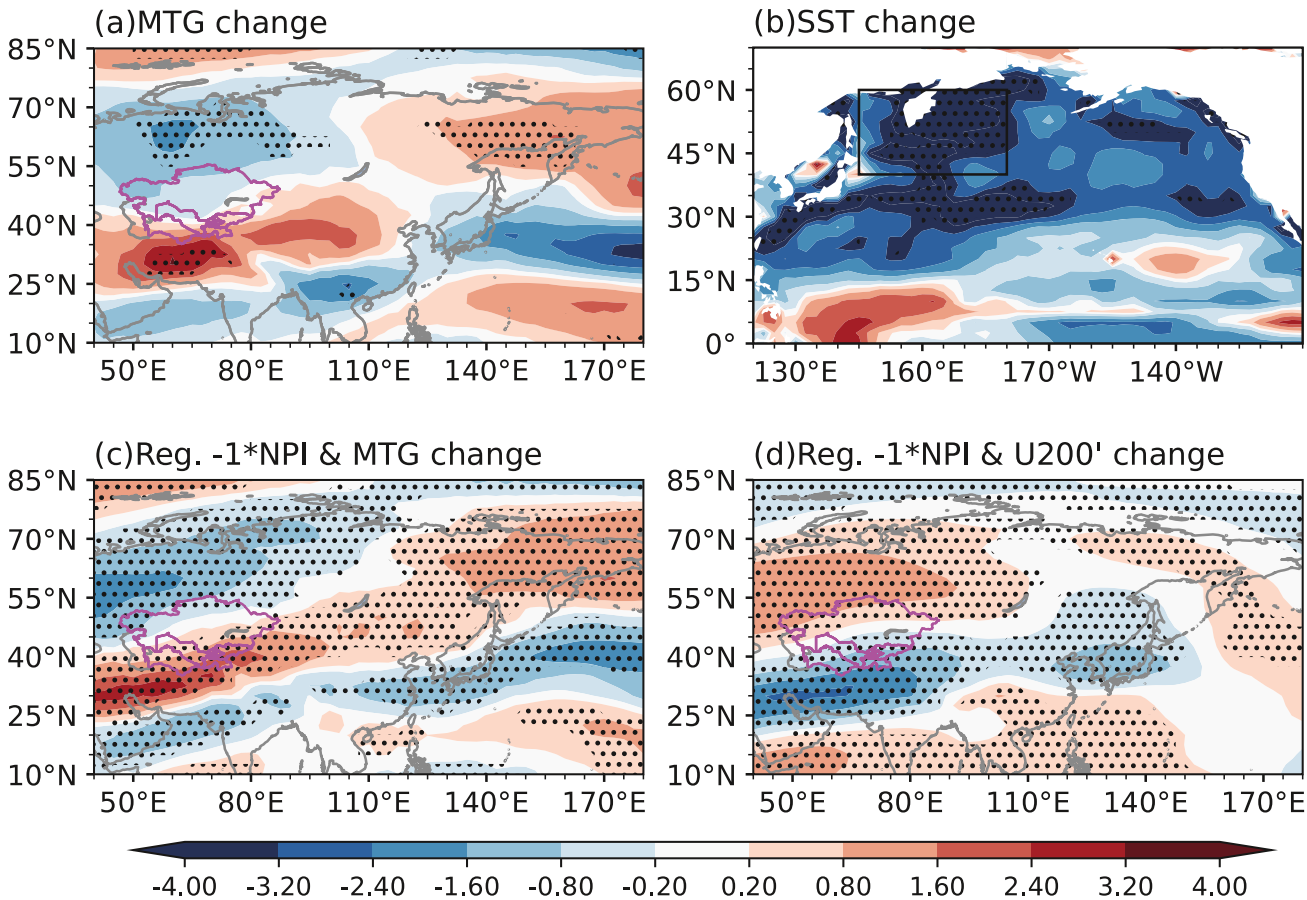

Figure 4. Inter-model regression of changes in winter (a) vertically integrated meridional temperature gradient (MTG) (units: 10^{-8} m^{-1}, shading) and (b) sea surface temperature (units: K K^{-1}, shading) with winter Central Asian precipitation. The black box indicates the key cold region of North Pacific index (NPI) (145°–180°E, 40°–60°N). The regression of changes in winter (c) vertically integrated MTG (units: 10^{-8} m^{-1}, shading) and (d) 200-hPa zonal wind (units: 10^{-1} m s^{-1} K^{-1}, shading) with the opposite value of NPI. The solid dots indicate 90% confidence level.

further examine the main processes in the surface energy budget (detailed in Text S4 in Supporting Information S1). The negative anomalies of R_{LU} over Northwestern Pacific (Figure S8a in Supporting Information S1), indicative of cooling SST anomalies, are well explained by the R_{LD}, as well as LH, which exhibits a similar spatial pattern and magnitude (Figures S8b, S8d and S8g in Supporting Information S1). The pronounced cooling over the key region of the NPI is partially offset by increased SH and OHT, with a slight compensation from R_S (Figures S8c and S8e–g in Supporting Information S1). The similar spatial distribution but opposing values between OH T and LH in this region imply an interaction between these processes (Figures S8d and S8f in Supporting Information S1). Specifically, higher SSTs driven by positive OHT changes may be balanced by increased LH released into the atmosphere, resulting in surface cooling.

4. Conclusion and Discussion

In this study, we investigate the inter-model uncertainty in the projection of precipitation in CA, especially in winter, using outputs from 25 CMIP6 models. We also explore the physical linkages between these uncertainties and variations in upper-level jet streams and North Pacific SSTs. The CMIP6 models well reproduce the climatological WCAP, yet significant inter-model uncertainties persist in future projection. The WCAP exhibits a homogenous wetting trend under global warming, with the primary source of inter-model spread stemming from the dynamic component of vertical moisture advection. The enhanced ascent in the troposphere over CA is further attributed to the intensified EAPJ and weakened EASJ through positive relative vorticity advection and warm temperature advection. The physical mechanisms behind the out-of-phase variation between two westerly jets are

explored subsequently. Cooling SSTs in the North Pacific induce a dipole MTG pattern over CA, promoting an enhanced EAPJ and a weakened EASJ. This out-of-phase variation in jet intensity favors stronger ascendance, thereby contributing to increased wetting in CA through enhanced vertical moisture transport (Figure S9 in Supporting Information S1).

This study illustrates that the North Pacific SSTs may be responsible for the inter-model uncertainty of WCAP projection through modulating the MTGs across the Eurasian continent. The future modulation of North Pacific SST cooling on westerly jet. also complements the previous study (Liu et al., 2022), suggesting that cooling in the Northwestern Pacific may have different impacts under historical versus future scenarios (Figure S10 in Supporting Information S1). Apart from North Pacific SSTs, both the EASJ and EAPJ are also influenced by Atlantic and tropical Pacific SST conditions, as well as by mutual influences between the two jets. These drivers may either reinforce or counteract each other (Liu et al., 2021; Woollings et al., 2010; Xue & Zhang, 2016), highlighting the need for future research to fully understand their impacts on WCAP projections. Moreover, this study identifies uncertainties in projecting North Pacific SST as stemming from discrepancies in how climate models simulate surface energy balance in the region. These discrepancies are potentially linked to biases in cloud cover simulations, which can significantly affect the accuracy of SST projections. Addressing these biases is crucial for improving model reliability. Future research could focus on refining cloud cover simulations and employing techniques such as emergent constraints to correct these biases, ultimately narrowing the uncertainty of precipitation projections in arid CA.

Conflict of Interest

The authors declare no conflicts of interest relevant to this study.

Data Availability Statement

The monthly precipitation data sets include GPCC, CRU, and Udel are accessed from https://opendata.dwd.de/climate_environment/GPCC/full_data_monthly_v2022/10/, https://crudata.uea.ac.uk/cru/data/hrg/cru_ts_4.07/cruts.2304141047.v4.07/pre/, and https://downloads.psl.noaa.gov/Datasets/udel.airt.precip/, respectively. CMIP6 data sets (detailed in Table S1 in Supporting Information S1) could be directly downloaded from https://aims2.llnl.gov/search/cmip6. All relevant codes used in this study are available upon request from the corresponding authors.

Acknowledgments
We sincerely thank the anonymous reviewers for their insightful comments, which have greatly improved the quality of this manuscript. This work is funded by the National Natural Science Foundation of China (42141019 and 42261144687).

References

Bothe, O., Fraedrich, K., & Zhu, X. (2011). Precipitation climate of Central Asia and the large-scale atmospheric circulation. *Theoretical and Applied Climatology*, *108*(3–4), 345–354. https://doi.org/10.1007/s00704-011-0537-2

Chen, F., Yu, Z., Yang, M., Ito, E., Wang, S., Madsen, D. B., et al. (2008). Holocene moisture evolution in arid central Asia and its out-of-phase relationship with Asian monsoon history. *Quaternary Science Reviews*, *27*(3–4), 351–364. https://doi.org/10.1016/j.quascirev.2007.10.017

Enomoto, T. (2004). Interannual variability of the Bonin high associated with the propagation of Rossby waves along the Asian jet. *Journal of the Meteorological Society of Japan*, *82*(4), 1019–1034. https://doi.org/10.2151/jmsj.2004.1019

Folland, C. K., Rayner, N. A., Brown, S. J., Smith, T. M., Shen, S. S. P., Parker, D. E., et al. (2001). Global temperature change and its uncertainties since 1861. *Geophysical Research Letters*, *28*(13), 2621–2624. https://doi.org/10.1029/2001gl012877

Guo, H., Bao, A., Chen, T., Zheng, G., Wang, Y., Jiang, L., & De Maeyer, P. (2021). Assessment of CMIP6 in simulating precipitation over arid Central Asia. *Atmospheric Research*, *252*, 105451. https://doi.org/10.1016/j.atmosres.2021.105451

Hall, R., Erdélyi, R., Hanna, E., Jones, J. M., & Scaife, A. A. (2015). Drivers of North Atlantic Polar Front jet stream variability. *International Journal of Climatology*, *35*(8), 1697–1720. https://doi.org/10.1002/joc.4121

Huang, A., Zhou, Y., Zhang, Y., Huang, D., Zhao, Y., & Wu, H. (2014). Changes of the annual precipitation over central Asia in the twenty-first century projected by multimodels of CMIP5. *Journal of Climate*, *27*(17), 6627–6646. https://doi.org/10.1175/JCLI-D-14-00070.1

Jiang, J., & Zhou, T. (2021). Human-induced rainfall reduction in drought-prone northern central Asia. *Geophysical Research Letters*, *48*(7). https://doi.org/10.1029/2020gl092156

Jiang, J., Zhou, T., Chen, X., & Zhang, L. (2020). Future changes in precipitation over Central Asia based on CMIP6 projections. *Environmental Research Letters*, *15*(5), 054009. https://doi.org/10.1088/1748-9326/ab7d03

Jiang, J., Zhou, T., Wang, H., Qian, Y., Noone, D., & Man, W. (2020). Tracking moisture sources of precipitation over central Asia: A study based on the water-source-tagging method. *Journal of Climate*, *33*(23), 10339–10355. https://doi.org/10.1175/jcli-d-20-0169.1

Lee, S., & Kim, H.-k. (2003). The dynamical relationship between subtropical and eddy-driven jets. *Journal of the Atmospheric Sciences*, *60*(12), 1490–1503. https://doi.org/10.1175/1520-0469(2003)060<1490:TDRBSA>2.0.CO;2

Liao, Z., & Zhang, Y. (2013). Concurrent variation between the East Asian subtropical jet and polar front jet during persistent snowstorm period in 2008 winter over southern China. *Journal of Geophysical Research: Atmospheres*, *118*(12), 6360–6373. https://doi.org/10.1002/jgrd.50558

Lioubimtseva, E., & Cole, R. (2006). Uncertainties of climate change in arid environments of Central Asia. *Reviews in Fisheries Science*, *14*(1–2), 29–49. https://doi.org/10.1080/10641260500340603

Lioubimtseva, E., & Henebry, G. M. (2009). Climate and environmental change in arid Central Asia: Impacts, vulnerability, and adaptations. *Journal of Arid Environments*, *73*(11), 963–977. https://doi.org/10.1016/j.jaridenv.2009.04.022

Liu, A., Huang, Y., & Huang, D. (2022). Inter-model spread of the simulated winter surface air temperature over the Eurasian continent and the physical linkage to the jet streams from the CMIP6 models. *Journal of Geophysical Research: Atmospheres*, *127*(22), e2022JD037172. https://doi.org/10.1029/2022JD037172

Liu, A., Xue, D., Chen, X., & Huang, D. (2024). Emergent constraints on the future East Asian winter surface air temperature changes. *Environmental Research Letters*, *19*(6), 064050. https://doi.org/10.1088/1748-9326/ad4a91

Liu, X., Grise, K. M., Schmidt, D. F., & Davis, R. E. (2021). Regional characteristics of variability in the northern Hemisphere wintertime polar front jet and subtropical jet in observations and CMIP6 models. *Journal of Geophysical Research: Atmospheres*, *126*(22). https://doi.org/10.1029/2021jd034876

Masson-Delmotte, V., Zhai, P., Pirani, A., Connors, S. L., Péan, C., Berger, S., et al. (2021). Climate change 2021: The physical science basis. Contribution of working group I to the sixth assessment report of the intergovernmental panel on climate change 2.

Pang, X., Wu, B., & Ding, S. (2023). Strengthened connection between meridional location of winter polar front jet and surface air temperature since the mid-1990s. *Climate Dynamics*, *60*(9), 3211–3224. https://doi.org/10.1007/s00382-022-06495-8

Peng, D., Zhou, T., Zhang, L., Zhang, W., & Chen, X. (2019). Observationally constrained projection of the reduced intensification of extreme climate events in Central Asia from 0.5°C less global warming. *Climate Dynamics*, *54*(1–2), 543–560. https://doi.org/10.1007/s00382-019-05014-6

Qiu, H., Zhou, T., Chen, X., Wu, B., & Jiang, J. (2024). Understanding the diversity of CMIP6 models in the projection of precipitation over Tibetan plateau. *Geophysical Research Letters*, *51*(3). https://doi.org/10.1029/2023gl106553

Ranasinghe, R., Wu, C. S., Conallin, J., Duong, M., & Anthony, E. J. (2019). Disentangling the relative impacts of climate change and human activities on fluvial sediment supply to the coast by the world's large rivers: Pearl River Basin, China. *Scientific Reports*, *9*(1), 9236. https://doi.org/10.1038/s41598-019-45442-2

Rivera, J. A., & Arnould, G. (2020). Evaluation of the ability of CMIP6 models to simulate precipitation over Southwestern South America: Climatic features and long-term trends (1901–2014). *Atmospheric Research*, *241*, 104953. https://doi.org/10.1016/j.atmosres.2020.104953

Schiemann, R., Lüthi, D., Vidale, P. L., & Schär, C. (2008). The precipitation climate of central Asia—Intercomparison of observational and numerical data sources in a remote semiarid region. *International Journal of Climatology: A Journal of the Royal Meteorological Society*, *28*(3), 295–314. https://doi.org/10.1002/joc.1532

Schneider, U., Hänsel, S., Finger, P., Rustemeier, E., & Ziese, M. (2022). GPCC full data monthly product version 2022 at 0.5°: Monthly land-surface precipitation from rain-gauges built on GTS-based and historical data.

Sun, J., Wu, S., & Ao, J. (2016). Role of the North Pacific sea surface temperature in the East Asian winter monsoon decadal variability. *Climate Dynamics*, *46*(11), 3793–3805. https://doi.org/10.1007/s00382-015-2805-9

Varis, O. (2014). Resources: Curb vast water use in central Asia. *Nature*, *514*(7520), 27–29. https://doi.org/10.1038/514027a

Wang, X. f., & Huang, H. l. (2011). The causation analysis of persistent heavy rain over southern China during May—June 2010. *Meteorological Monthly*.

Woollings, T., Hannachi, A., & Hoskins, B. (2010). Variability of the North Atlantic eddy-driven jet stream. *Quarterly Journal of the Royal Meteorological Society*, *136*(649), 856–868. https://doi.org/10.1002/qj.625

Wu, H.-m., Huang, A.-n., He, Q., & Zhao, Y. (2013). Projection of the spatial and temporal variation characteristics of precipitation over Central Asia of 10 CMIP5 models in the next 50 years. *Arid Land Geography*, *36*(4), 669–679.

Xu, H., Wang, T., & Wang, H. (2024). The Interdecadal Pacific Oscillation is responsible for the linkage of decadal changes in precipitation and moisture in arid central Asia and the humid Asian monsoon region during the last millennium. *Climate of the Past*, *20*(1), 107–119. https://doi.org/10.5194/cp-20-107-2024

Xue, D., & Zhang, Y. (2016). Concurrent variations in the location and intensity of the Asian winter jet streams and the possible mechanism. *Climate Dynamics*, *49*(1–2), 37–52. https://doi.org/10.1007/s00382-016-3325-y

Yao, J., Chen, Y., Chen, J., Zhao, Y., Tuoliewubieke, D., Li, J., et al. (2021). Intensification of extreme precipitation in arid Central Asia. *Journal of Hydrology*, *598*, 125760. https://doi.org/10.1016/j.jhydrol.2020.125760

Yao, M., Tang, H., Huang, G., & Wu, R. (2024). Interdecadal shifts of ENSO influences on spring central Asian precipitation. *npj Climate and Atmospheric Science*, *7*(1), 194. https://doi.org/10.1038/s41612-024-00742-x

Yin, J., & Zhang, Y. (2021). Decadal changes of east Asian jet streams and their relationship with the mid-high latitude circulations. *Climate Dynamics*, *56*(9), 2801–2821. https://doi.org/10.1007/s00382-020-05613-8

Yu, Y., Chen, X., Malik, I., Wistuba, M., Cao, Y., Hou, D., et al. (2021). Spatiotemporal changes in water, land use, and ecosystem services in Central Asia considering climate changes and human activities. *Journal of Arid Land*, *13*(9), 881–890. https://doi.org/10.1007/s40333-021-0084-3

Zhang, J., Chen, Z., Chen, H., Ma, Q., & Teshome, A. (2020). North Atlantic multidecadal variability enhancing decadal extratropical extremes in boreal late summer in the early twenty-first century. *Journal of Climate*, *14*.

Zhang, M., Chen, Y., Shen, Y., & Li, B. (2019). Tracking climate change in Central Asia through temperature and precipitation extremes. *Journal of Geographical Sciences*, *29*(1), 3–28. https://doi.org/10.1007/s11442-019-1581-6

Zhao, Y., Yu, X., Yao, J., & Dong, X. (2018). Evaluation of the subtropical westerly jet and its effects on the projected summer rainfall over central Asia using multi-CMIP5 models. *International Journal of Climatology*, *38*(S1), e1176–e1189. https://doi.org/10.1002/joc.5443

Zhou, X., Liu, F., Wang, B., Xiang, B., Xing, C., & Wang, H. (2019). Different responses of east Asian summer rainfall to El Niño decays. *Climate Dynamics*, *53*(3–4), 1497–1515. https://doi.org/10.1007/s00382-019-04684-6